공학석사 학위논문

Wind Tunnel Experiment and Development of Thermodynamic Model for Dry Snow Accretion on a Heated Surfaces

가열 표면에 대한 건형 착설의 풍동 실험 및 열역학적 모델 개발

2022년 8월

서울대학교 대학원

항공우주공학과

서송현

Wind Tunnel Experiment and Development of Thermodynamic Model for Dry Snow Accretion on a Heated Surfaces

가열 표면에 대한 건형 착설의 풍동 실험 및 열역학적 모델 개발

지도 교수 김 규 홍

이 논문을 공학석사 학위논문으로 제출함

2022 년 6 월

서울대학교 대학원

항공우주공학과

서송현

서송현의 공학석사 학위논문을 인준함

2022 년 6 월

위 원 장 이 관 중 (인)

부위원장 김 규 홍 (인)

위 원 이 복 직 (인)

Abstract

In railway vehicle, snowpack on bogie and the underframe caused by snow accretion can result in a various type of damage along with performance degradation. To acquire reliable data for characteristic of snow accretion on railway vehicles, effect of surface heat transfer caused from mechanical or electrical subsystems should be considered. In this paper, wind tunnel experiment and modeling of dry snow accretion on a heated surface were carried out to estimate characteristics of dry snow accretion that occur in sub-freezing temperature with using a small climatic wind tunnel. The experiments were conducted with respect to surface heat flux regarding atmospheric conditions such as air temperature, wind speed and snow flux. Including growth rate, sticking efficiency and liquid water content, measurement about accreted snow properties was systemically applied to analyze the dry snow accretion on a heated surface. The experiments show a strong influence of surface heat flux on the snow accretion process. Sticking efficiency of dry snow can be correlated with the liquid water content of accreted snow layer and meteorological parameters. Accreted snow layer shed from surfaces when liquid water content lies slightly above then 40%. The sticking efficiency and liquid water content of accreted snow layer were estimated through a thermodynamic model which considers the effects of convective cooling and evaporation of liquid water inside the accreted snow. The modeling results was analyzed and cross-validated with the experimental measurements, and it has 0.97 and 0.92 of adjusted R-squared value for sticking efficiency and liquid water content, respectively. The experimental and analytical findings of this study can be considered as extend of existing knowledge about snow accretion phenomena to dry snow. Therefore, this study can be further extended to wet snow as well as dry snow.

Keyword: Snow accretion phenomena, Dry snow, Wind tunnel experiment, Surface heat transfer, Sticking efficiency, Liquid water content.

Student Number: 2020-29410

Contents

List of Figure

List of Table

Nomenclature

Abbreviations

LWC	-	liquid water content
PIV	-	particle image velocimetry

Latin symbols

A	-	area [m^2]
C_p	-	specific heat of air at constant pressure [J/kg K]
C_i	-	specific heat of ice [J/kg K]
D	-	characteristic length [m]
G	-	growth rate [$kg/m^2/s$]
h	-	convective heat transfer coefficient [W/m^2 K]
I	-	electrical current [A]
L_m	-	latent heat of fusion of ice [J/kg]
L_v	-	latent heat of water [J/kg]
m	-	mass [kg]
n	-	number of snow block introduce to snowfall simulator [-]
P	-	joule heating effect [W]
p	-	pressure [Pa]
q	-	heat flux [W/m^2]
R	-	resistance [Ω]
S	-	snow flux [$kg/m^2/s$]
T	-	temperature [℃]
U	-	wind speed [m/s]
V	-	test model input voltage [V]

Greek symbols

α	-	melting rate [-]
β	-	sticking efficiency [-]
ϵ	-	molecular weight ratio of dry air and water vapor [-]
η	-	test model heating efficiency [-]
κ	-	thermal conductivity [W/m K]
λ	-	liquid water content of snow [-]
ν	-	kinematic viscosity [m^2/s]
τ	-	snowfall duration [s]
ϕ	-	relative humidity [-]
ω	-	absolute humidity [-]

Subscripts

a	-	air
cd	-	condensation
cv	-	convection
ev	-	evaporation
e	-	experimental
eq	-	equilibrium
eff	-	effective accretion
i, l, s	-	ice, liquid water, snow
mean	-	mean value
mt	-	melting
net	-	net of control volume
o	-	initial state
s.b.	-	snow block
surf	-	surface
t.s.	-	test section
v	-	vapor

Superscripts

$+/-$	-	heating/cooling effect to the control volume

Dimensionless Groups

Nu	-	Nusselt number
Pr	-	Prandtl number
Re	-	Reynolds number
Sc	-	Schmidt number

1. Introduction

1.1. Introduction

When train passing through the snow cover area, the wind induced by train passage cause snow particles to bounce and drift, and it accreted to the bogie and the underframe. Especially, in the case of dry snow, which is generated in sub-freezing temperature, snow easily swirls around the vehicle and generate snow smokes larger due to its characteristic which light and consists of very fine particle [**1**]. Consequently, these particles easily attach to those regions where surface heat transfer is presence such as car body, air intake and disc brake. The resulting snow packs not only degrade the performance, but also cause various types of damage to vehicles and track [**2**]. In recent study it has been assessed that window glass damage at high-speed train can be attributed to snow accretion under the car body [**3**].

Figure 1 Snow smoke from the wind induced by trains passage [**1**].

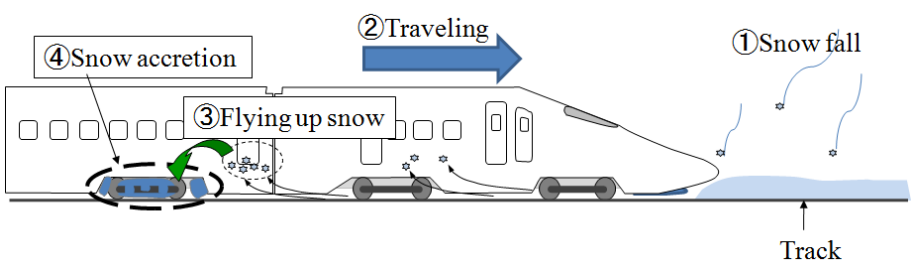

Figure 2 Process of snow accretion on a railway vehicle [**2**].

1.2. Study background

For the railway vehicles, because of its complex geometry and large scale, indoor experiment with using climatic wind tunnel are costly expensive and inefficient to clarify the influence of the meteorological parameters. In-rail tests are possible but continuous conditions at which snow accretion occurs cannot be encountered repeatably or easily measured. Therefore, most of study about snow accretion phenomena in real-scale vehicles are mainly conducted by the numerical simulations [**4**-**8**]. These types of programs are composed with a two-phase solver (flowfield and particle trajectory), and results will be varied depending on how to modeling the interfacial sticking mechanism between surface and particles. Trenker [**4**], by adopting local friction velocity which is indicator for particles being dispersed from surface [**9**], presumed that the threshold friction velocity can holds as a criterion whether particles stick to a surface or being reflected. Xie [**5**] and Liu [**6**] simulate the snow distribution by Lagrange particle trajectory model, then they assessed the regions where the snow accumulation occurs without consideration of particle-wall interaction. Yoon [**7**] imitate the snow as supercooled water droplet in the recalescence stage of the flow field [**10**], then establish the sticking rate of impinged particles by correlating the liquid water content of supercooled water droplet. Cai [**8**] simulate the result of impact between snow particles and surface based on the snow particle deposition model [**11**,**12**] which using the critical capture velocity and the critical wind friction velocity as a criterion determining whether particles rebound, detach and deposit on the surface.

In the aforementioned studies, the limitation of modeling about snow-wall interaction is distinct; sticking fractions should be known empirically at a given condition and thus it is inflexible to changing meteorological conditions; not all colliding particles lead to adhesion and its levels varies in local geometric and thermodynamic conditions; phenomena of accretion of snow and supercooled water droplet are physically different. Given the current dearth of experimental data about railway snow accretion, the bounds of conditions which is in a good degree of accuracy is limited. Moreover, the available information about thermodynamic parameters which has meteorological dependency is not enough to determine the formation of snow accretion in a railway vehicle.

1.3. Study objectives

Applicable analytical models for snow accretion have been well-studied on electric transmission lines and power network, based on numerous field observations data and indoor experiments results [**13-17**]. However, most of the models are derived from empirical correlations of the cylindrical geometries; studies on wet snow conditions are predominant; temperature effect is frequently omitted [**18**], so there are some limitations to its application to railway vehicles. Since bonding mechanism during the collision mainly comes from the refreezing process or hydrogen bonds of liquid water inside the snow particles [**19**], generally, sticking of dry snow in the sub-freezing is out-of-consideration in their studies because of its lack of initial water content. Moreover, studies about surface heat transfer related to snow accretion and icing are interested in how much it melts, not how much it makes accrete.

In the present study, a wind tunnel experiment and modeling the dry snow accretion on a heated surface is established in a thermodynamic approach to provide a mechanism for the necessary physical process at any condition of dry snow accretion in railway vehicles. The experiment is systematically applied to different conditions of air temperature, wind speed, snow flux and surface heat flux to assess their influence. In order to characterize the sticking fraction of colliding snow particles, experiment include not only measurement of accreted snow mass but also liquid water content. In addition, the relation between meteorological parameters, surface heat flux and snow properties are modelled and cross-validated with experiment data to clarify the dependency of sticking fraction of snow. Then, explicit equation of sticking efficiency is derived, which can be used as a criterion of accreted fraction of snow impinging to surfaces.

2. Experimental facilities and setup

All the presented experiments including wind tunnel experiments and synthesis of artificial snow were executed using cold experimental facilities installed in the Korean National University of Transportation. These facilities have been used for various experiments related to snowfall phenomena [**20**,**21**]. Cold laboratory is composed with two separate climate chambers to facilitate environment control. One is for operating wind tunnel for snow accretion experiment (Fig. **3**) and the other for producing artificial snow particles. Air temperature inside each chamber is controlled by the air conditioning system from -30 to 30 ℃. Because of presence of snow inside the cold laboratory, air humidity was kept in 80～90%.

A particle image velocimetry (PIV) investigation was adopted to set the motion of flow and snowflakes. The light sheets are generated by a dual cavity flash-pumped Nd:YAG lasers (DualPower, Dantec Dynamic®) separated in time by 100 ～ 200 μs at 15 Hz (no. 1 in Fig. **3**). Light sheeted particle was captured with a 29M pixel high speed double frame camera (FlowSense EO, Dantec Dynamic®) (no. 2 in Fig. **3**). The measurement was executed in a vertical plane, along the centroidal axis of the test section. For more details about measurement principles of PIV may refer [**22**,**23**].

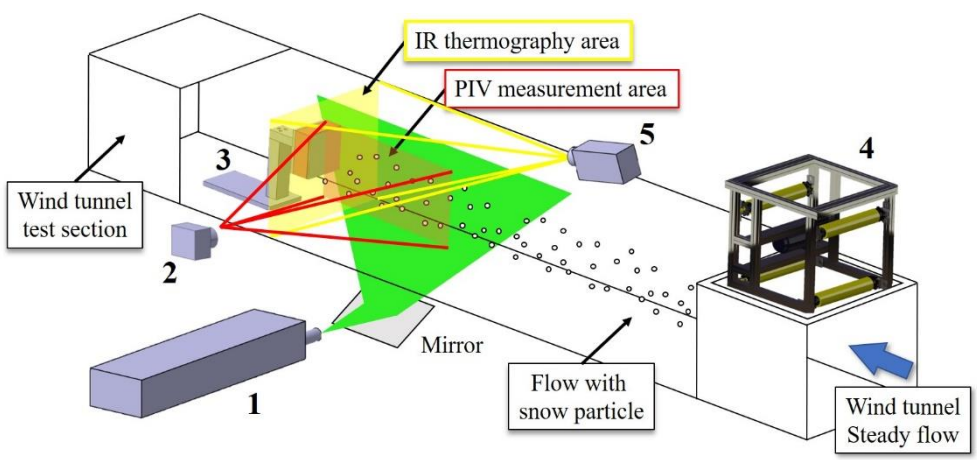

Figure 3 Overview of the experimental setup. The setup was equipped with Nd:YAG laser with light sheet optics (1) and High speed camera (2) for PIV measurement. Test model (3) and snowfall simulator (4) were designed for snow accretion experiment. IR camera (5) were placed above the test section to acquire the thermography.

2.1. Wind tunnel

The wind tunnel is open end type with a 3.0 m long, 0.3 m width and 0.3m height clear acrylic test section. The wind speed can be set from 0 to 30 m/s, and turbulence intensity at 30 m/s is less than 0.8%. Since temperature scope of design conditions of wind tunnel is 10 to 40 ℃, wind speed data was calibrated using PIV measurements. Changing speed of wind tunnel driving motor from 100 to 1000 RPM, wind speed in test section was measured by PIV. The accuracy of the wind speed in test section is determined by the standard error of linear fit equation which of the PIV measurement data. The final wind speed data used for this experiment are accurate to within 0.53%.

2.2. Artificial snow and simulate snowfall

In this experiment, snow was produced with a custom-built snow maker in a cold laboratory set at -25 ◦C. The machine designed after the same principles as the used by [**24**]. Water vapor provided from warm water bath condensed into nylon strings (see Fig. **4**a). Each synthesized snow particle basically has a dendritic and needles structures in its crystal as shown in Fig. **4**b. The size of the snow particles ranges from 0.5 mm to 5.0 mm, approximately. This type of snow has been used for various experiments as a good substitute for natural snow [**25**,**26**]. Artificial snow was kept in a container every 300 g as a block (Fig. **5**), and moved to wind tunnel testing chamber. Since the presented experiments were targeted at dry snow accretion and compared with dry snow accretion modeling. Snow block container were preserved in a sub-freezing temperature same as wind tunnel experiments condition. Care was taken to avoid additional heat transfer to snow block container.

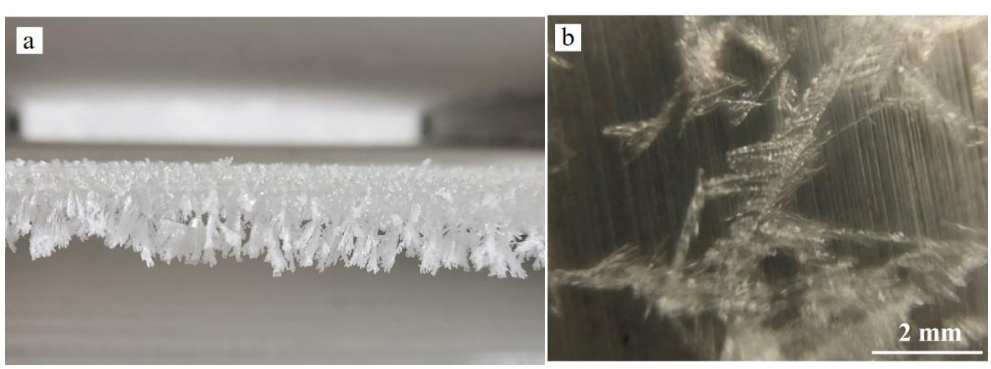

Figure 4 Synthetic snow crystals growing on nylon wires (a) and dry snow sample for experiment (b).

Figure 5 Snow block used for simulation snowfall.

Snowfall in wind tunnel test section was simulated by snowfall simulator (no. 4 in Fig. **3** and Fig. **6**). To shred snow block and inject snow flake into the air flow, snow block was ground by a rotating mesh which is rotated at a constant speed by a servo-gear assembly. This system was installed at the distance from the wind tunnel test section above to introduce snowfall into the air flow directly.

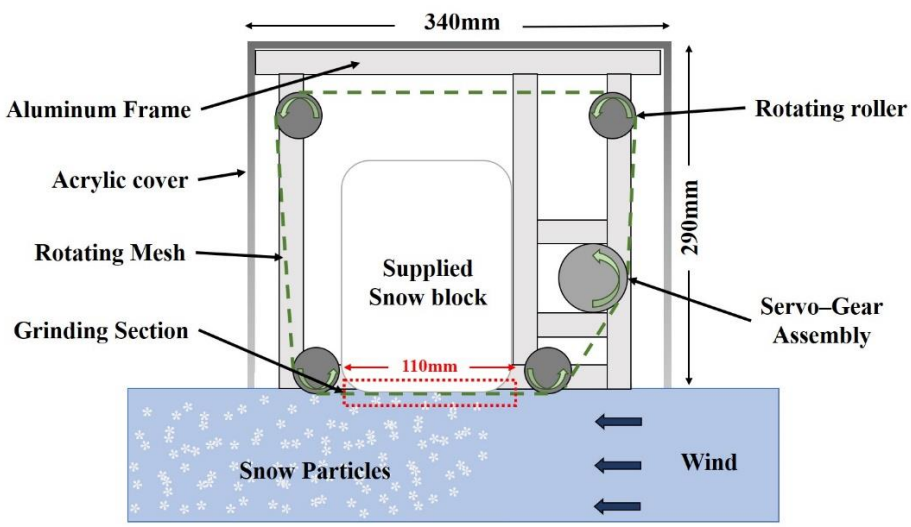

Figure 6 Detailed configurations of snowfall simulator.

2.3. IR camera

Infrared thermography was adopted for temperature measurement and heat flux assessment (no.5 in Fig. **3**). During the experiment, the surface temperature of the test model and the snow layer was measured with an infrared camera (testo 890, Testo®). The size of the thermography image is 640 × 480 pixels and temperature resolution of the cameras is 0.1 ℃ with an accuracy within 2% of the measured value. The emissivity of the test model for thermography was calibrated based on thermocouple (JIS TX-FF 0.32 K-type) data. The data acquisition system was mounted in a PC equipped with a post-processing software and images were acquired at a 33 Hz rate.

2.4. Test model

A schematic configuration of the test model and side view where the support is separated is shown in Fig. **7**. The test model consist of 0.1 m width and 0.1 m height aluminum vertical plate (1) covered with a thin layer of paint that exhibits a high emissivity for heat flux assessment and silicone heater pad (2) powered by DC power supplier, thereby forming a heating in a frontal surface. To minimize heat losses, insulation (3) was placed behind the heater pad. Custom made support (4) was used to set snowflake impingement surface normal and centroid to the wind tunnel flow. Test model and support are assembled with hand screw bolt to easily initiate the measurement of snow properties right after the experiments.

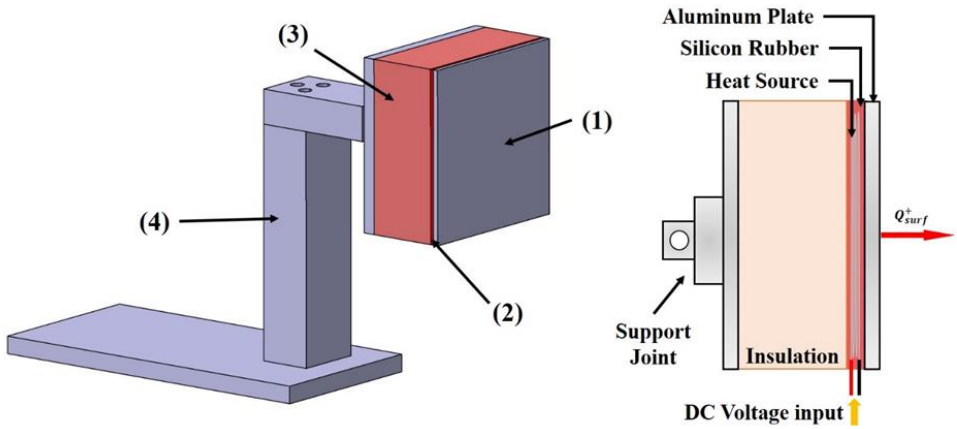

Figure 7 Schematic configuration of test model.

2.4.1. Heat flux data reduction

In general, heating effect P by the ideal resistive joule heating with resistance R and electric current I is $P = RI^2$. But for a real world, the heating effect is influenced by the heating efficiency, and it is not a universal constant, but rather a variable depending on environmental state [**27**]. In this study, to applied the surface heat transfer adequately, heating efficiency of test model is systematically examined with using IR thermography.

The heat flux assessment using thermography requires a temperature measurement and is deduced from it with a dedicated data reduction method [**28**]. In the present work, a data reduction method based on the theory of the 1-D convective heat transfer into a vertical plane with cross-flow was used. For these method, desired steady flow was established in the test section with the test model and without snowflake inside; the DC power (Voltage input in Fig. **7**) was then applied to the heater pad until surface temperature reach steady state. After about 10 minutes, surface temperature was then measured by IR camera. Surface temperature was measured in every experiment case with changing voltage from 1.0 to 10.0 V.

From convective heat transfer relation, surface temperature deduced to surface heat flux (q_{surf}) by:

$$q_{surf} = h(T_{surf,mean} - T_a) \tag{1}$$

where T_a is air temperature and $T_{surf,mean}$ is mean value of test model surface temperature measured by IR thermography. h is convective heat transfer coefficient which about flat plates perpendicular to the freestream, and it can be calculated from [**29**]:

$$h = \frac{\kappa_a Nu}{D} = 0.667 Re_D^{1/2} Pr_a^{1/3} \frac{\kappa_a}{D} \tag{2}$$

$$Re_D = \frac{DU}{\nu_a} \tag{3}$$

where κ_a is thermal conductivity of air, Nu is Nusselt number, D is characteristic length (herein height of test model), Re_D is Reynolds number, Pr_a is Prandtl number, U is wind speed and ν_a is kinematic viscosity of air.

Thermal properties are used in film temperature value (average value of air temperature and surface temperature).

Based on Ohm's law ($V = IR$), heat flux from electrical resistance heating can be fitted into quadratic equation with applied voltage and it intersects with the beginning of the 0 V ($q_{sruf} = 0$). Therefore, the relation of the surface heat flux according to the applied voltage can be obtained by a 2nd curve fit equation like below,

$$q_s = \eta V^2 \tag{4}$$

where V is test model input voltage and η is test model heating efficiency calculated by Eqs. **1**, **2** and **4** from 2nd curve fit equation. The value of η used in snow accretion experiments to control the surface flux at each air temperature T_a = -3, -5, -7 ℃ is 9.581, 9.670, 9.482, respectively. The accuracy of heat flux is determined by the standard error of 2nd curve fit equation of reduced data. The final surface heat flux according to input voltage are accurate to within 8.9%.

3. Experimental method

3.1. Experimental conditions

For the wind tunnel experiments, the air temperature was set to sub-zero temperature T_a = -3, -5, -7 ℃ at constant wind speed U = 7 m/s in order to aim a dry snow condition with the value of liquid water content of snow can be assume 0%.

In addition, experiments with three different wind speed U = 5, 7, 9 m/s at constant air temperature T_a = -5 ℃ were executed to investigate the influence of the wind speed on the characteristic of accreted snow layer. The distance from the snowfall simulator to test model was adjusted to distribute snowflake identically over the cross section of test section depending on the wind speed. Because of the sedimentation speed of the different snow particles and of their respective trajectories, the intensity of the snowfall through the test section is, of course, approximately constant but not identical throughout the test section [**15**]. The distance was set by visual observation, then precisely adjusted with using PIV mapping technique throughout the selected region. The final location of test model from snowfall simulator is 70 cm at 5 m/s, 141 cm at 7 m/s, 208 cm at 9 m/s, respectively.

Surface heat flux of test model was set from 150 W/m^2 to condition which accreted snow layer shed from test model surface with intervals of 150 W/m^2. Under conditions described above, flow with snow particle in a test section was created by continuous injection of 3 snow block into the snowfall simulator over 6 minutes. In this case, snow flux is 0.02778 kg/m^2/s which calculated as follow,

$$S = \frac{n m_{\text{s.b.}}}{\tau A_{\text{t.s.}}} \tag{5}$$

where n is number of snow block introduce to snowfall simulator, and $m_{\text{s.b.}}$ is the mass of snow block, and τ is snowfall duration, and $A_{\text{t.s.}}$ is cross section area of test section.

In addition, to observing effect of influence of the snow flux, high snow flux condition was conducted at air temperature T_a = -5 ℃ and wind speed U = 7 m/s. In this case, snow flux was adjusted by only changing speed of motor

of snowfall simulator, thereby snowfall duration τ is 180 seconds and snow flux is 0.05556 kg/m^2/s.

In Table **1**, details about experiment conditions are tabulated. After in this paper, experiment condition will be indicated with combination of experiment case and number, which #2-8 is represent air temperature T_a= -5 ℃, wind speed U = 5 m/s and snow flux S = 0.02778 kg/m^2/s with surface heat flux q_{surf} = 1200 W/m^2.

Table 1 Details of experiment condition

Exp. Case	T_a [℃]	U [m/s]	S [kg/m^2/s]	τ [s]	Exp. No.	q_{surf} [W/m^2]
1	-5	7	0.02778	360	1	150
2	-5	5	0.02778	360	2	300
3	-5	9	0.02778	360	3	450
4	-3	7	0.02778	360	4	600
5	-7	7	0.02778	360	5	750
6	-5	7	0.05556	180	6	900
					7	1050
					8	1200
					9	1350
					10	1500
					11	1650

3.2. Experimental procedure

Wind tunnel experiment of dry snow accretion on a test model and measuring properties of accreted snow layer were performed in the following process.

1. Install the test model inside the wind tunnel test section at the location of targeted wind speed.

2. Set the targeted air temperature and wind speed in the wind tunnel. Turn on the power supplier and input target voltage to generate a heat flux in test model front surface.

3. In order to avoid excessive initial surface heat transfer and create snow accretion under steady heat transfer state, snowfall simulator was initiated when surface temperature reaches to equilibrium temperature T_{eq} (temperature at which latent heat and total heat transfer to accreted snow layer are balanced). Initial equilibrium temperature on surface can be calculated by Eqs. **1** and **16** under the condition of $q_{surf} + q_{cv} + q_{ev} = 0$, which will be explained later, and it is T_{eq} = 3.1, 4.6, 4.9 ℃ at T_a = -3, -5, -7 ℃, respectively.

4. After snowfall in the test section, turn off the power supply and remove test model from wind tunnel immediately in order to prevent additional heat transfer to accreted snow layer.

5. Take a photograph of snow layer for the assessment of effective accretion area. In case of low surface heat flux, such as #1-2, #2-1, #3-2, et cetera, snow accretion did not occur in all areas. In this case, photograph data was shaded to visualize the snow then effective accreted area was measured along the edge of snow layer (see Fig. **8**).

6. Isolate test model from supporter, and measure the weight of the accreted snow layer and liquid water content. For the measurement of liquid water content, melting type snow water content meter was used [**30**].

The time required to perform experiment procedure 4 to 6 took less than 2

minutes, and author confirmed that influence of these time was negligible to changing the order of the measured value. Experiment was conducted repeatedly with changing surface heat flux, and last experiment number for each case is #1-9, #2-11, #3-8, #4-8, #5-9, #6-11, respectively.

Although, experiment was conducted under the conditions that the surface heat flux is 1 step higher than the above-mentioned (#1-10, #2-12, #3-9, #4-9, #5-10, #6-12). These results were not included in this paper. Because the snow layer shed from the test model surface in the middle of the experiment or in the process of removal from test section for measurement, it was not possible to measure their properties.

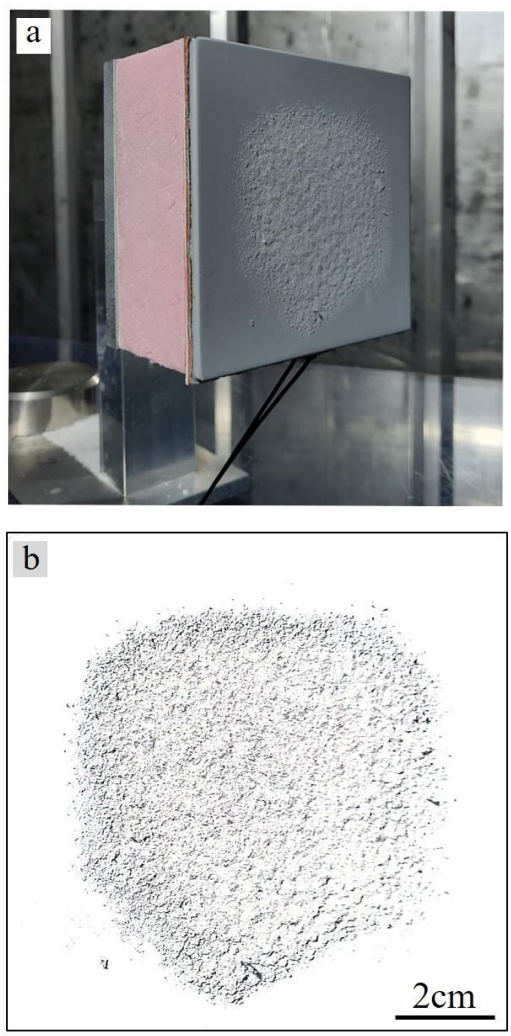

Figure 8 Example of the measurement of the effective accretion area. Photograph data of accreted snow layer of #2-2 case (a) and shaded image for assessment (b).

4. Wind tunnel experiment result

4.1. Effective accretion area

Since the surface heat flux was reduced from average surface temperature. Regions where forming a temperature which is lower than freezing can be existed locally, and snow cannot be accreted on those regions. Therefore, assessment of effective accretion area, not using test model frontal area, is vital for dry snow accretion modeling process.

In Fig. **9**, comparison of effective accretion area respect to the surface heat flux with the different experiment cases is presented together with test model frontal area value. In cases of #5-2 and surface heat flux is 150 W/m^2, except for #4-1, snow was not accreted on the surface or not much enough to determine edge of snow cover area, and result of these cases were not included in Fig. **9**. It can be observed that the effective accretion area is affected by not only air temperature but also wind speed. As surface heat flux increases, snow covered area reaches to test model frontal area asymptotically. The center of the test model surface is stagnation point, where convection cooling effect is lower than the edge. So, the local surface heat flux in stagnation point is greater than that of edge. Therefore, as shown in, Fig. **8** snow accretion only occurs around the flow stagnation region owing to insufficient heat exchanges.

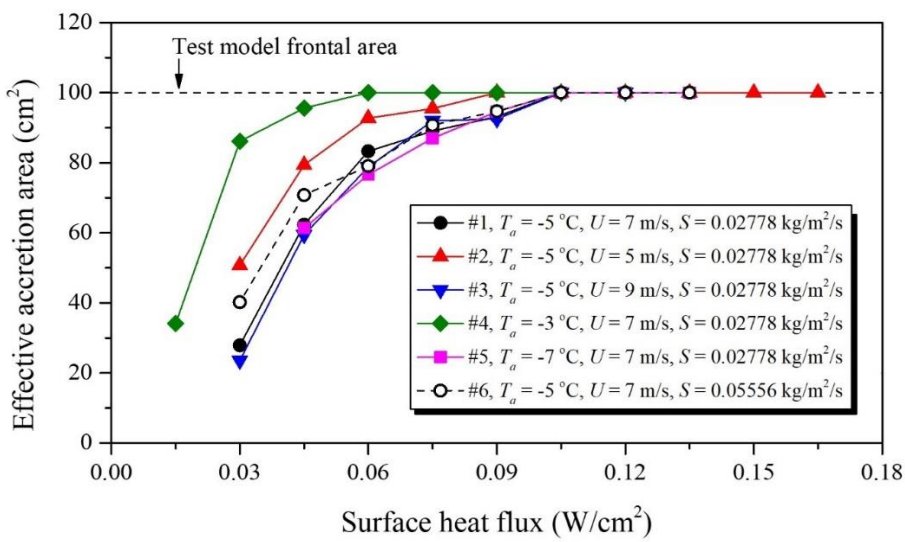

Figure 9 Effective accretion area respect to the surface heat flux with the different experiment cases.

4.2. Accreted snow mass on test model

For the quantitative analysis about characteristic of dry snow accretion, the growth rate and sticking efficiency are introduced. Growth rate G (kg/m^2/s) is accreted snow mass per unit area with respect to time, and calculated as follow,

$$G = \frac{m_s}{A_{\text{eff}}\tau} \tag{6}$$

where A_{eff} is effective accretion area which is measured for each experiment condition. Growth rate represents the rate of change of accreted mass on surfaces. Because of the aerodynamic reasons (bouncing of the snow particles by the air flow) and mechanical reasons (break of impinging snowflakes), all the snow particles are not accreted on surfaces. This aspect can be parameterized by sticking efficiency β (%), and calculated as follow,

$$\beta = \frac{G}{S} \tag{7}$$

where S is snow flux which is calculated from Eq. **5**. Sticking efficiency represents the ratio of accreted snow particles to snow impinging the surface.

In Fig. **10**, measured growth rate and sticking efficiency according to surface heat flux at the constant snow flux S = 0.02778 kg/m^2/s are presented. For the same snow flux cases, sticking efficiency can be calculated from just dividing growth rate with snow flux. Thus, sticking efficiency was presented together in second Y axis. It can be observed that snow was not accreted at all in some cases, such as #1-1, #2-1, #3-1, #5-1, #5-2, and accreted snow mass is significantly small at the heat flux around 300 W/m^2. This is because not only initial surface temperature is below the equilibrium temperature, but also mechanical cohesive force of dry snow is low. However, as the increase of the surface heat flux, it is observed that growth rate and sticking efficiency are increased almost linearly. It means that the surface heat flux largely affect the accreted snow mass. Heat exchanges between surface and impinging snow particles make water content on surface by melting, and it make dry snow adhere. LWC inside the accreted snow layer is increased according to increase of surface heat flux, and as a result, rate of accretion is increased. This relation between liquid water content and accretion rate is reasonable,

because dry snow transform into wet snow by heat exchange [**17**,**31**]. The aforementioned tendency is observed regardless of experiment conditions, and it indicates that surface with a small heat flux make dry snow to accrete rather than de-snow effect. As the surface heat flux is increased, of course, accreted snow layer shed from surface because of going out of adhesive forces by metamorphosis of snow structure. But the level of surface heat flux is varied in every experiment case. The quantitative analysis about shedding conditions will be provided in the following sections with measured liquid water content.

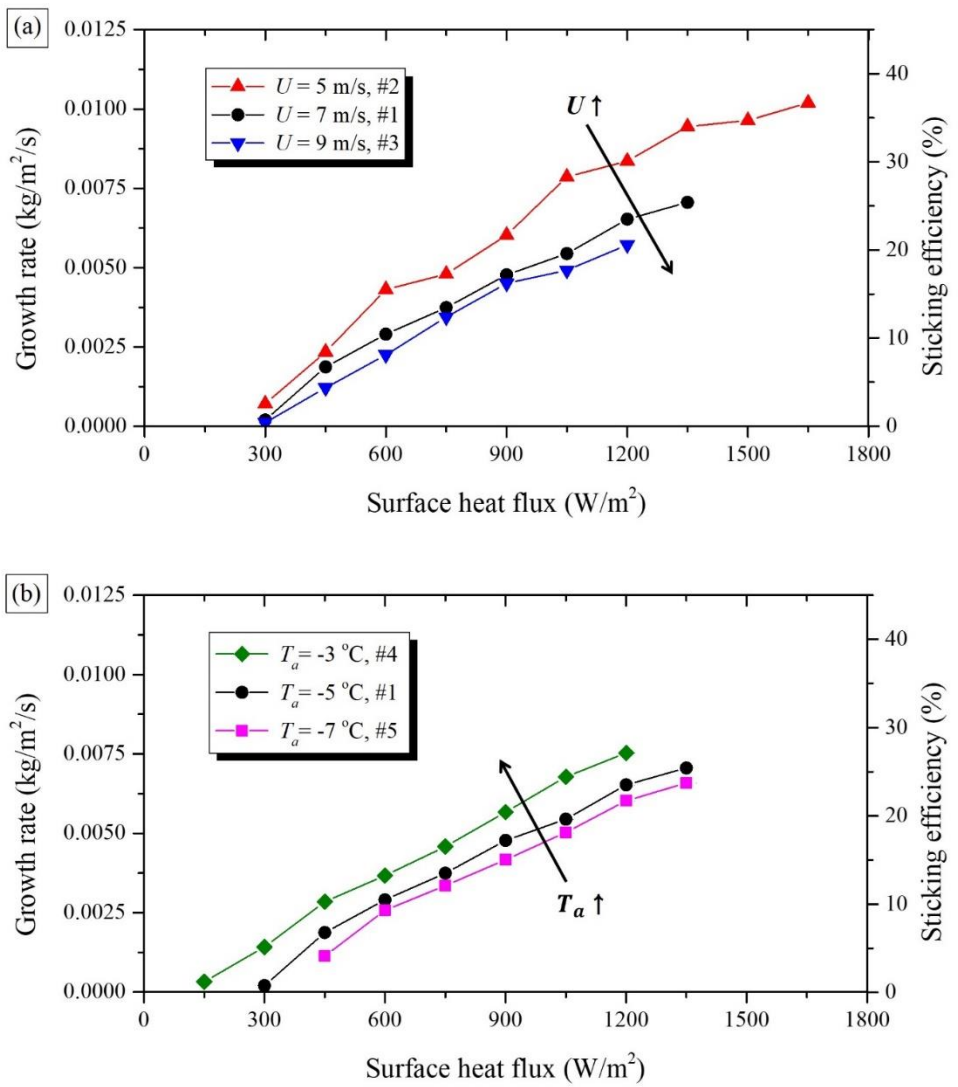

Figure 10 Measured growth rate and sticking efficiency according to surface heat flux in different wind speed (a) and air temperature (b).

In the comparison of wind speed from 5 to 9 m/s (Fig. **10**a), accreted snow mass is decreased according to increase of wind speed. Snow particles with higher velocities, owing to their higher inertial forces, can overcome the interfacial force and re-bound from surface more efficiently [**19**]. And this relation between accretion rate and wind speed becomes feeble at high wind speeds [**16**]. Furthermore, increased impinging speed leading snow particle to saltate from the surface more actively [**12**,**32**]. Thus, accreted snow mass decrease respect to increase of wind speed, and deviation between #1 and #3 is smaller than that of #1 and #2. In the comparison of air temperature from -3 to -7 ℃ (Fig. **10**b), accreted snow mass is increased according to increase of air temperature. This is resulted from that increase of air temperature make cooling effect become more restrained. Accordingly, LWC of snow surface is increased, leading to increase of accretion rate.

In Fig. **11**, measured growth rate and sticking efficiency according to surface heat flux in different snow flux is presented. As shown in Fig. **11**a, it is confirmed that growth rate has higher value at intense snow flux conditions. However, even though snow flux was doubled from 0.02778 to 0.05556 $kg/m^2/s$, total mass of accreted snow is not doubled. The aforementioned is confirmed apparently in Fig. **11**b by observing sticking efficiency has lower value at higher snow flux conditions. If the dry snow is accreted and mixed with wet surfaces, LWC of snow surface will decreased since mass fraction of ice inside the accreted snow layer is increased. This effect become intense when the number of impinging snow particles per unit area is increased (which means increase of snow flux). Consequently, at higher snow flux condition, it is considered that sticking efficiency is reduced due to the decrease of LWC at a given surface heat flux.

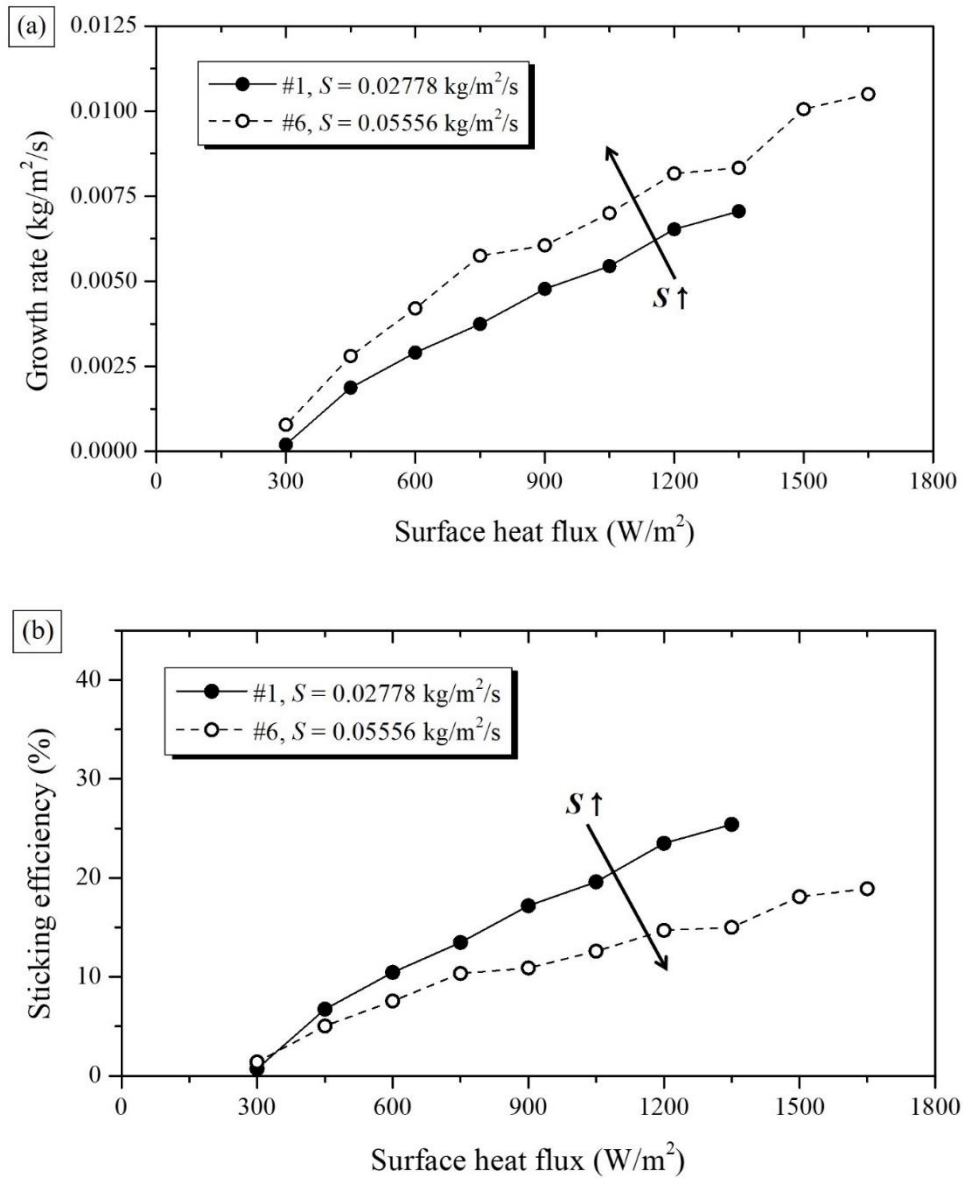

Figure 11 Measured growth rate (a) and sticking efficiency (b) according to surface heat flux in different snow flux.

4.3. Liquid water content of accreted snow

For the analysis in snow accretion phenomena, assessment of liquid water content is vital, since the adhesion strength of snow greatly affects by the capillary force due to liquid water and cohesive forces between ice particles generated through the metamorphosis of snow [**33,34**]. LWC can be expressed as mass fraction of water inside the accreted snow as,

$$\lambda = \frac{m_l}{m_s} \tag{8}$$

where m_l is the weight of liquid water in the accreted snow layer, and m_s is the total weight of the accreted snow layer.

In Fig. **12**, measured liquid water content of accreted snow layer according to surface heat flux with respect to varying the meteorological conditions U, T_a and S is presented together with the 40% of shedding criterion. It is obvious that value of LWC is increased proportionally according to the surface heat flux. Thereby, it can be confirmed that analyzing the accreted snow mass by correlate its LWC in previous section is reasonable. It is observed that measured LWC of last experiment No. (#1-9, #2-11, #3-8, #4-8, #5-9, #6-11) is at around 40% regardless of the experiment cases. Considering that the experiment was performed up to one step higher than the suggested surface heat flux value, it can be presumed that LWC will be lies slightly above then 40% under the condition which the de-snow occur. In the wet snow conditions, when the air temperature is above freezing, once the LWC of accreted snow reached to 40%, cohesive forces are conspicuously reduced so that the snow deposit, and shed [**35-37**]. Therefore, these results suggest that snow start to shed when LWC of snow exceeds 40% regardless of conditions which initial state of snow (wet or dry) and thermal state of surface (adiabatic or isothermal).

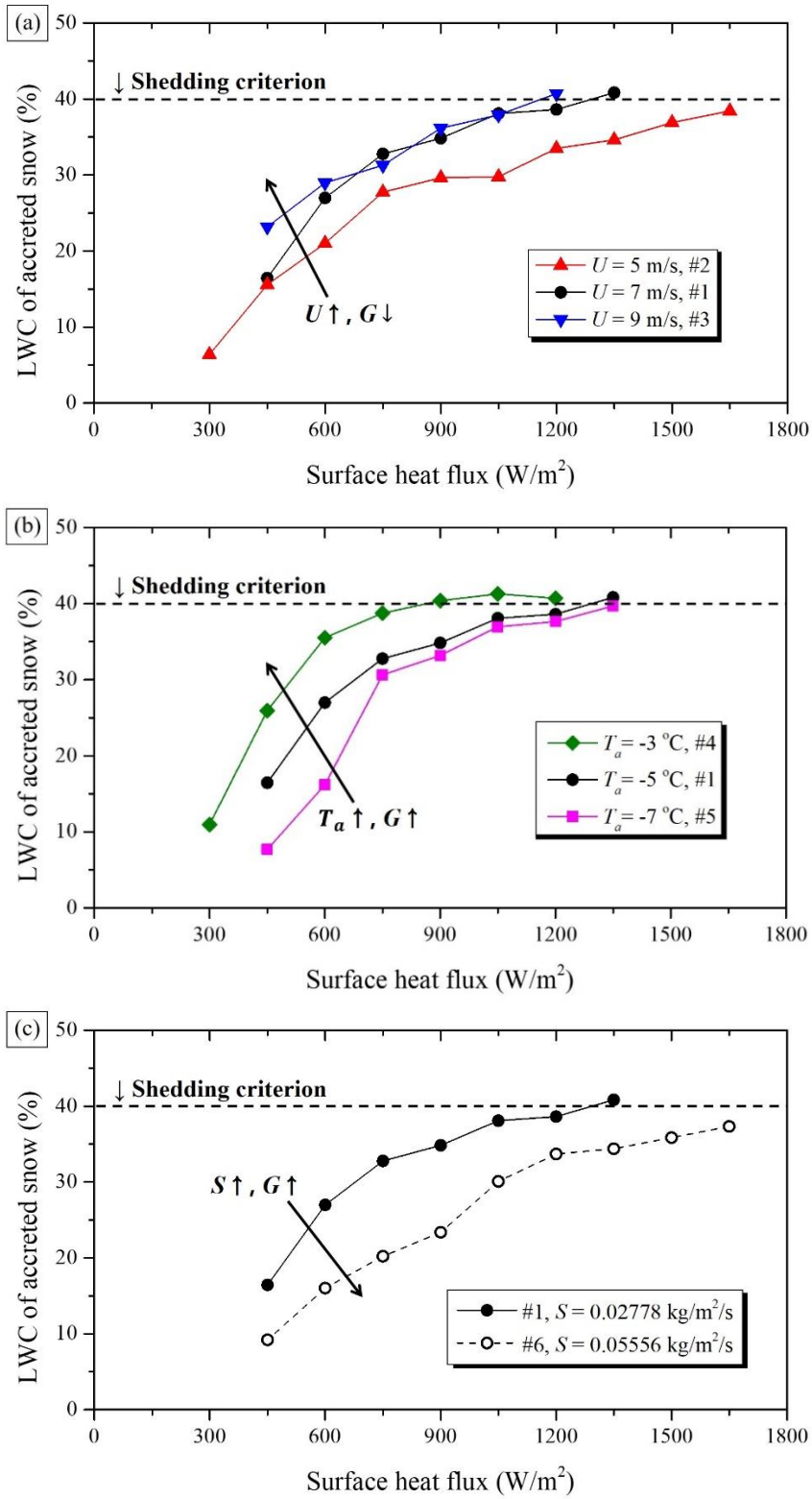

Figure 12 Measured liquid water content according to surface heat flux in different wind speed (a), air temperature (b) and snow flux (c).

By comparing the LWC with wind speed in Fig. **12**a, #2 deviate from the #1 and #3. As mentioned in section 4.2, reduced wind speed restricted the bouncing effect leading to increase of accretion rate. This increased amount of accreted snow mass decreases the values of LWC at a given surface heat flux. Furthermore, these correlation between accretion rate and LWC can be seen in Fig. **12**c, herein LWC is decreased due to increase of snow flux result in an increase of accreted snow mass.

By comparing the LWC with air temperature in Fig. **12**b, LWC is increased respect to increase of air temperature. The lower the temperature, the active the cooling effect by convection. Thus, melting rate of accreted snow is restrained which leading to decrease of LWC. Furthermore, water is a substance that can be kept at liquid state at temperatures as low as -35 ℃ because of its relatively high specific heat [**14**]. Therefore, even at sub-freezing temperatures, the dry snow will contain some LWC and it will be greater at higher temperatures. It is considered that this difference makes #4 to slightly deviate from the #1 and #5.

5. Modeling of dry snow accretion

5.1. Thermodynamic considerations

In this modeling, radiative heat transfer, sublimation of snow, transformation of ice crystals and mass transfer by evaporation or condensation of the water vapor are omitted due to their insignificant influence [**38-40**]. In Fig. **13**, schematic of main heat exchanges in snow accretion process are presented. In snow accretion phenomena, various types of heat exchanges occur, and it can be parameterized in unit area by meteorological parameters. In the previous section, the surface heat flux of test model (q_{surf}) was parameterized by Eq. **4**. The mass transfer, which the rate of accreted snow mass, is parameterized as a growth rate by Eqs. **6** and **7** with using G, S, β. The parametrization of significant heat exchanges will be provided in the following section.

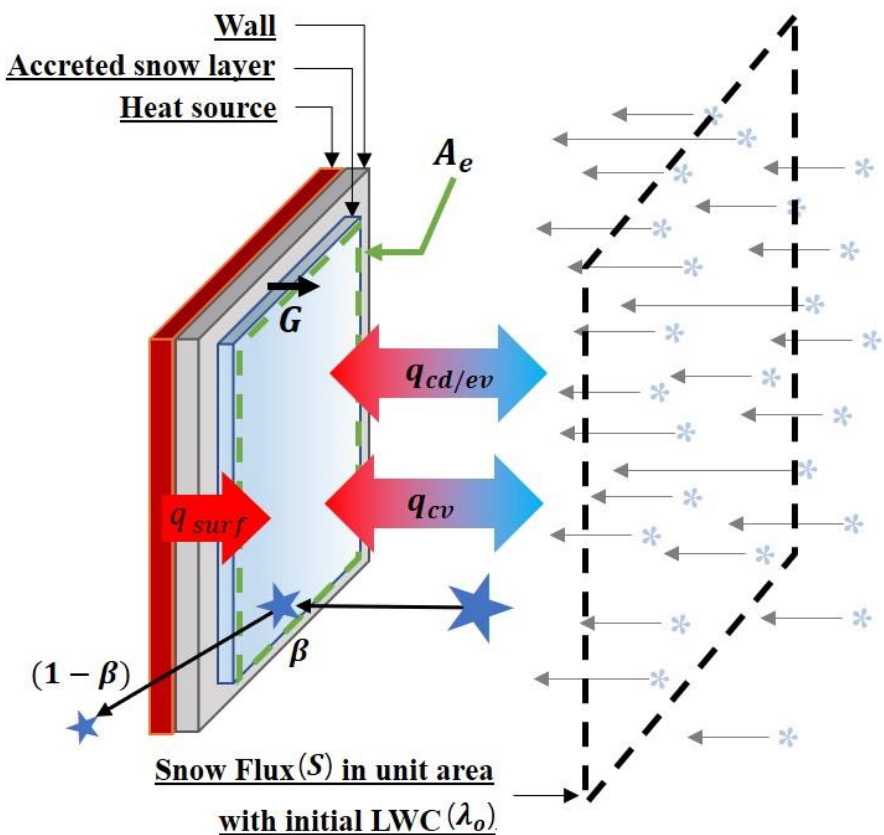

Figure 13 Schematic of main heat exchanges in snow accretion process.

5.1.1. Convection

The heat transfer from forced convection can be expressed as follows:

$$q_{cv} = h(T_a - T_s) \tag{9}$$

where h represents the convective heat transfer coefficient of air and T_s is the surface temperature of accreted snow. Considering the surface of accreted snow as a flat plate, h can be obtained by Eq. **2**. T_s can be assumed as 0 ℃, since the ice and water mixture is at a uniform temperature of 0 ℃. From the thermography data, author confirmed that surface temperature of the snow accretion region dropped to 0 ℃ immediately after the start of snowfall, and it was maintained throughout the experiment duration. Summarizing the above, convective heat flux reduces to following equation.

$$q_{cv} = 0.667 Re_D^{1/2} Pr_a^{1/3} \frac{\kappa_a}{D} T_a \tag{10}$$

It is note that Re is non-dimensional parameter that depend on wind speed and air properties in given geometric configurations. Therefore, q_{cv} has a unique value at given T_a and U.

5.1.2. Evaporation and condensation of water vapor

Although the mass transfer due to evaporation and condensation is insignificant, the heat exchange should be considered since the latent heat of water is relatively large. The heat flux from the evaporation and condensation of water can be expressed by [**15**]:

$$q_{ev/cd} = \frac{L_v}{C_p}\left(\frac{Pr_a}{Sc}\right)^{0.63} h\Delta\omega \tag{11}$$

where L_v is latent heat of water, C_p specific heat of air at constant pressure and Sc is Schmidt number of the air-water mixture at snow air interface (Sc = 0.605). $\Delta\omega$ is the difference in the absolute humidity between atmospheric water vapor and condensed phases water vapor on the accreted snow surface. This can be calculated as follow:

$$\Delta\omega = \epsilon\frac{\phi p_v^{T_a} - p_v^{0℃}}{p_a} \tag{12}$$

where ϵ is the ratio of the molecular weights of dry air and water vapor (ϵ = 0.622), ϕ is relative humidity and P_a is atmospheric pressure (P_a = 100 kPa). p_v^T is the saturation vapor pressure at given temperature T, and it can be estimated by [**41**]:

$$p_v^T = \exp\left(\frac{21.875T}{T + 265.5}\right) \tag{13}$$

Combining Eqs. **2**, **11**, **12** and **13**, $q_{ev/cd}$ can be calculated as a unique value for a given T_a, U and ϕ.

5.1.3. Melting of accreted snow

The snow flux (S) with initial LWC (λ_o) passes through the surface (A_{eff}), and the part of snow particles (β) are accreted on the surface (G) (see Fig. **13**). After impact, the various heat exchanges increase latent heat of snow, and creates the melting part (α) among the dry fraction ($1-\lambda_o$) inside the accreted snow layer. The accumulated heat flux due to the increase of latent heat and melting of snow are parameterized as follows:

$$q_{mt} = G(1-\lambda_o)\{L_m\alpha + C_i(0℃ - T_{o.s.})\} \tag{14}$$

where L_m is latent heat of fusion of ice, C_i is specific heat of ice and $T_{o.s.}$ is snow initial temperature. In dry snow conditions, initial LWC close to 0, so melting rate α becomes LWC of accreted snow layer λ. By assuming initial snow temperature is equal to air temperature, and combining Eq. **14** with Eq. **7** yields:

$$q_{mt} = \beta S(L_m\lambda - C_iT_a) \tag{15}$$

This expression suggests that q_{mt} can be estimated by measured value β and λ at a given experiment conditions *S,* T_a.

5.2. Modeling of accretion parameter in dry snow conditions

Considering the quasi 1-D steady heat flux through the effective accretion area, select a control volume, as shown in Fig. **14**. The accreted snow layer is thin enough, so, it is reasonable to assume that the heat flux only passing through the accrete snow layer in orthogonal direction. Performing an energy balance on the control volume yields the following equation.

$$q_{mt}^{+} = q_{surf}^{+} + q_{cv}^{-} + q_{ev}^{-} \tag{16}$$

denoted superscript + and - represent the heating and cooling effect to the control volume, respectively. q_{ev} is the heat flux by evaporation of water vapor, since the air stream is below-saturated at sub-freezing temperature ($\Delta\omega < 0$), there will be an evaporation process on the surface.

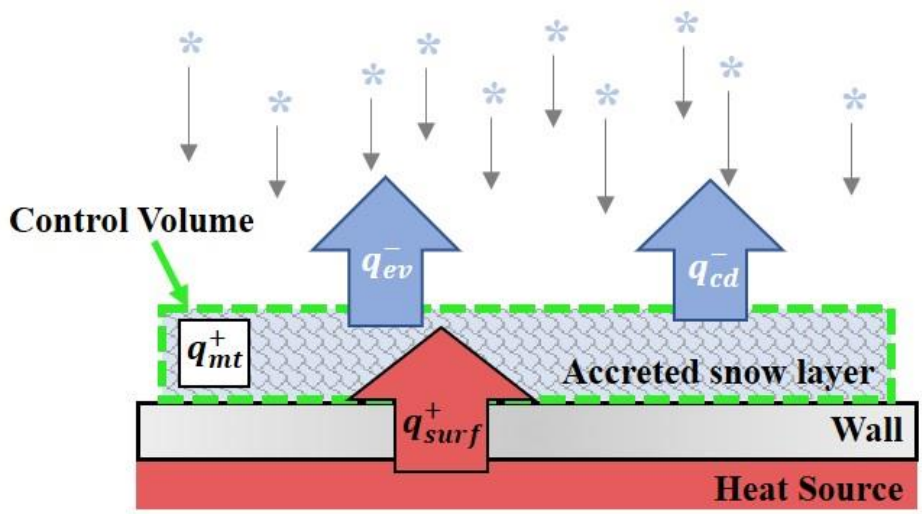

Figure 14 Frame work of dry snow accretion on heated surfaces.

Substituting Eq. **16** to Eqs. **10**, **11** and **15**, the heat flux through the control volume can be expressed as the following balanced equation.

$$\begin{aligned}\beta S(L_m\lambda - C_i T_a) &= q_{net} \\ &= q_{surf}^{+} + 0.667 Re_D^{1/2} Pr_a^{1/3} \frac{\kappa_a}{D} T_a + \frac{L_v}{C_p}\left(\frac{Pr_a}{Sc}\right)^{0.63} h\Delta\omega\end{aligned} \tag{17}$$

where q_{net} on the right-hand-side of the equation represent the net heat flux through the control volume, that is total heat supplied to the accreted snow layer.

In order to snow to accrete on surfaces continuously ($\beta > 0$), total heat supplied to accreted snow layer should be greater than 0. Therefore, the initial equilibrium temperature in the experiment conditions are calculated by Eqs. **1** and **16** under condition of $q_{mt} = 0$ (herein $T_{surf,mean}$ substitute to T_{eq}).

By equating right-hand-side of Eq. **17** and q_{net}, an explicit expression of sticking efficiency β and LWC λ are respectively derived,

$$\beta = \frac{1}{S}\frac{q_{net}}{L_m\lambda_e - T_a C_i} \tag{18}$$

$$\lambda = \frac{1}{L_m}\left(\frac{q_{net}}{\beta_e S} + C_i T_a\right) \tag{19}$$

where λ_e and β_e is the measured value from the experiments. It should be mentioned that q_{net} is only a function of q^+_{surf} at a given S, T_a, ϕ and U. Thus, at a given meteorological condition, sticking efficiency and liquid water content is increased proportionally to the increase of surface heat flux and decrease inversely with respect to increase of snow flux. Additionally, since the air temperature is sub-freezing ($T_a < 0$), decrease of air temperature leading sticking efficiency and liquid water content to decrease.

To demonstrate the accuracy of this model, sticking efficiency and LWC of 47 experiments points were computed by Eqs. **18** and **19**, and result are shown Fig. **15**. The correlation plot between measured and calculated value of sticking efficiency and LWC are shown in Fig. **15**a and Fig. **15**b, respectively. It may be seen that, although some differences occur, the overall correlation coefficient is 0.970 and 0.923. These relatively good predictive capability of models show that it is possible to estimate the sticking efficiency successfully with proper assumption of LWC of the accreted snow layer.

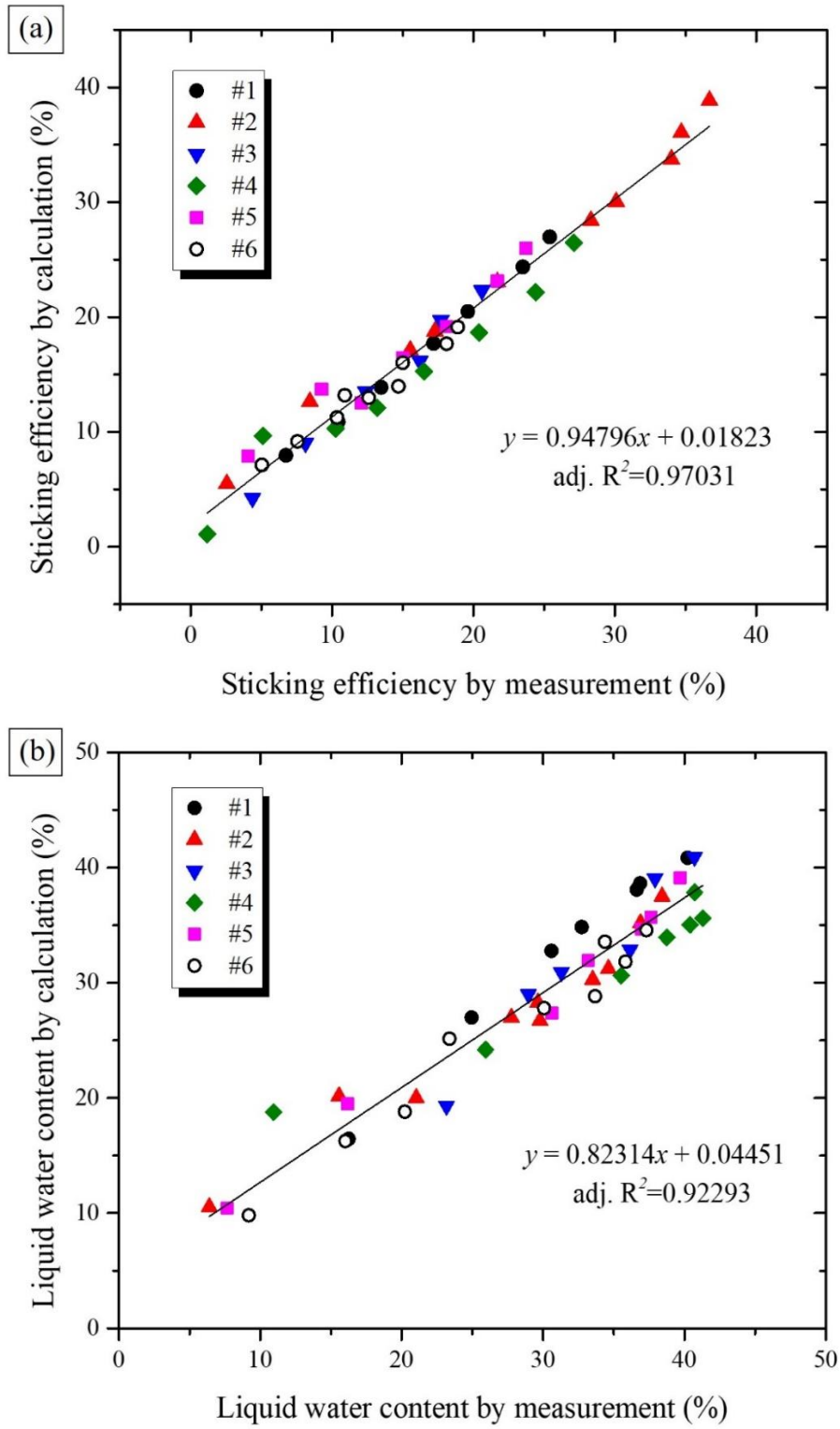

Figure 15 Correlation between experiment measurement and value calculated by the thermodynamic model for sticking efficiency (a) and Liquid water content (b). (n = 47)

5.3. Influence of the meteorological parameters on the sticking efficiency

In Fig. **16**, computed minimum sticking efficiency at different wind speed with respect to surface heat flux at a given meteorological conditions are presented. Herein λ_e is assumed to be 40%. As investigated in the section 4.3, the problem of the prediction of sticking efficiency is allied to the thermodynamic state of the accreted snow layer which is represented by LWC. Therefore, these two parameters (β and λ) should be determined simultaneously, not solely, and this problem can be identified in Eqs. **18** and **19**.

During the accretion process, the accreted snow layer undergoes a process of metamorphosis in which the snow particles form a snow pack held together by capillary forces and cohesive forces induced by water content. If the LWC is greater than 40%, the adhesive force is greatly reduced [**37**], and this make the snow layer to shed by the gravitational and aerodynamic force. Therefore, it can be considered that maximum LWC that the accreted snow layer can contain is 40%. Since the main reason for the increase in LWC in dry snow condition is the decrease of accreted snow mass, it is considered that estimating minimum sticking efficiency by maximized LWC is appropriate. Furthermore, literature findings suggest that limiting the sticking efficiency by shedding criterion is reasonable [**16**,**42**,**43**]. Hence, assuming the λ_e of Eq. **18** is 40%, the minimum sticking efficiency can be uniquely determined at a given meteorological conditions.

In Fig. **16**, the influence of the surface heat flux is confirmed to be quite distinct; the sticking efficiency is increased linearly to the surface heat flux. The effect of meteorological parameters on sticking efficiency can be identified by change of slope and deviation. As shown in Fig. **16**a, the higher the air temperature, the smaller the surface heat flux at which snow accretion begins ($\beta > 0$). At high air temperature ($T_a = 0℃$) the influence of wind speed U is very limited, but the effect of the wind speed becomes pronounced as the temperature become lower ($T_a = -5, -15$ ℃). As shown Fig. **16**b, the influence of snow flux is distinguished as a change of the slope. As the wind speed increases, the value of the surface heat flux at which snow accretion begins is increased, but slope coincides in the same snow flux; and the slope is inversely proportional to the snow flux. These trends of change in sticking

efficiency according to meteorological parameters is very consistent with experimental observations.

Since the present study was extend of existing knowledge about snow accretion phenomena to dry snow. The proposed equations to estimate sticking efficiency can be further applied to various cases with different snow types as well as different thermal state of surface.

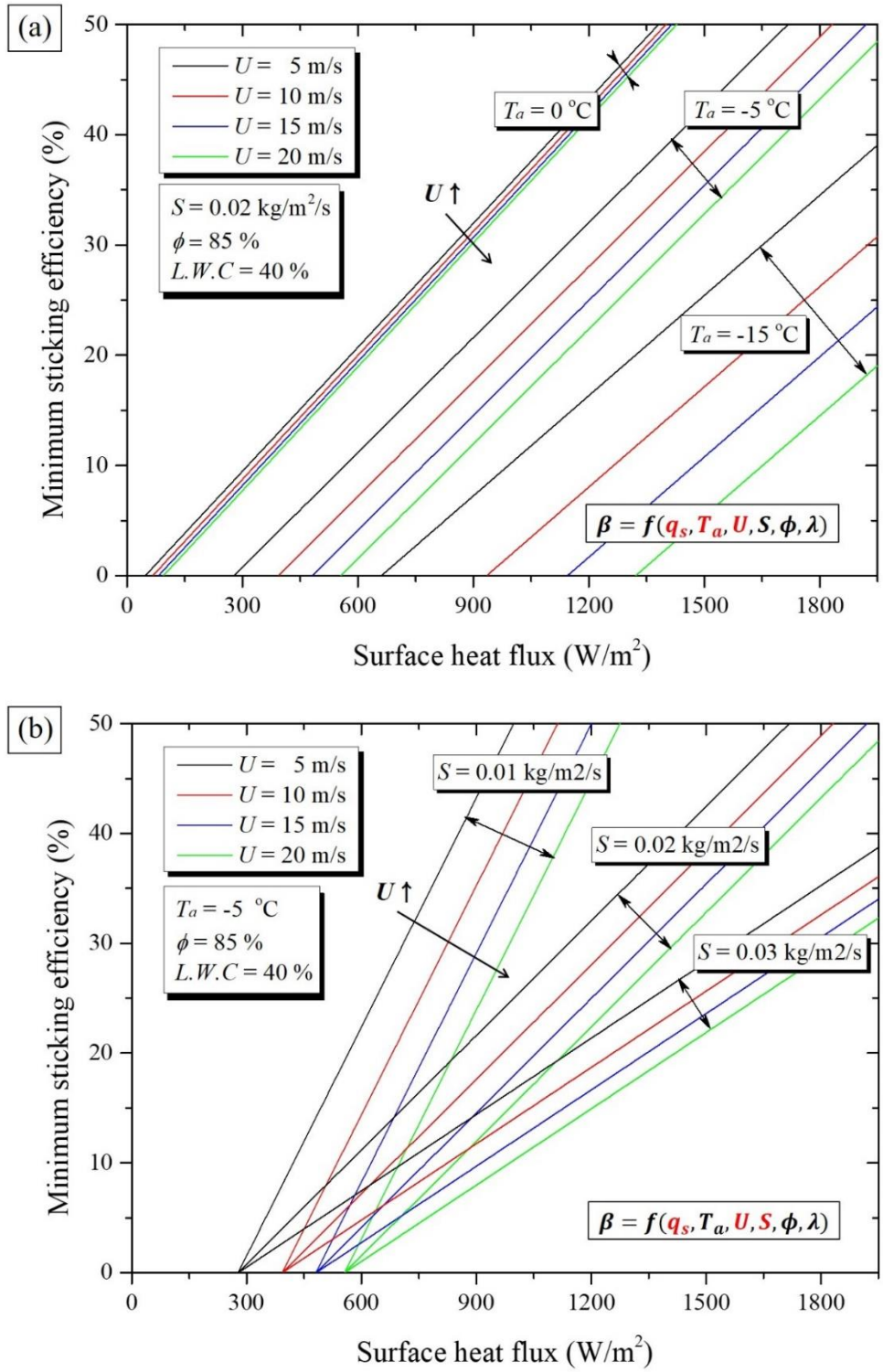

Figure 16 Minimum sticking efficiency at different wind speed with respect to surface heat flux at snow flux S = 0.02 kg/m^2/s (a) and air temperature T_a = -5 ℃ (b).

6. Conclusion

In the presented study, wind tunnel experiment and thermodynamic modeling for dry snow accretion on a heated surface were carried out. The test model was made to facilitate the accretion test, and tested in the cold laboratory. To investigate the influence of meteorological parameters, various experimental conditions was systemically established, and representative accretion parameters which is growth rate, sticking efficiency and liquid water content were measured. In the consideration of thermodynamic state of accretion process, dry snow accretion on heated surfaces was successfully modelled, and it was cross-validated with the experimental results. To estimate the influence of meteorological parameters, shedding criterion, which assumed liquid water content of accreted snow layer to be a 40%, is adopted, then minimum sticking efficiency was estimated through suggested model. As a result, the following conclusions is derived:

1. In dry snow conditions, the driving force of the snow accretion is the surface heat flux. The surface with a small heat flux allows dry snow to accrete rather than de-snow.

2. The growth rate and sticking efficiency, which is represent the rate of accreted snow mass, is varied depending on the air temperature and wind speed as well as the snow flux.

3. The liquid water content can be changed by not only the total heat supplied to the accreted snow layer but also the rate of accreted snow mass. Moreover, the criterion of shedding of accreted snow is determined by the 40% of LWC, and this result is shown regardless of initial state of snow and thermal state of surface as well as meteorological conditions.

4. Based on the thermodynamic considerations of the snow accretion process, numerical expression for representative accretion parameters, sticking efficiency and LWC, can be derived as a function of time-averaged parameters. Accuracy of the proposed equations is confirmed by the correlation plot between experimental measurements and computed value, and it is shown to be as 0.970 and 0.923 of adjusted-R^2 value for sticking efficiency and liquid water content, respectively.

5. In dry snow accretion, the lower limit of sticking efficiency can be uniquely determined under given experimental conditions by maximizing the LWC. Thereby the influence of the meteorological parameters can be identified as the change of slope and deviation in the linear correlations. Influence of air temperature and wind speed are proportional and inversely proportional to the sticking efficiency, respectively, and effect of wind speed becomes pronounced as the temperature increase. Finally, snow flux is distinguished as a change of the slope, and it effect inversely proportional to the sticking efficiency.

In the application of the proposed equations to estimate the sticking efficiency, heat transfer coefficient should be derived from given geometrical configuration. Therefore, in the numerical simulation method-based study, which can compute the local heat transfer coefficient, this method can be more utilized exquisitely.

Bibliography

[1] L. Kloow, M. Jenstav (2011) High-speed train operation in winter climate, Transrail Publication BVF5, 2.

[2] Y. Kamata, A. Yokokura (2019) Estimation Method of Snow Accretion Amount on Train Bogies, Proceedings of the IWAIS 2019 Reykjavik June 23-28.

[3] H. Kwon, et al., (2020) Study on relationship between weather condition and window glass damage by accreted snow for high-speed trains, Journal of the Korean Society for Railway 23(2), 135–142. doi: 10.7782/JKSR.2020.23.2.135.

[4] M. Trenker, W. Payer (2006) Investigation of snow particle transportation and accretion on vehicles, 24th Applied Aerodynamics Conference, 3648. doi: 10.2514/6.2006-3648.

[5] F. Xie, et al., (2017) Study of snow accumulation on a high-speed train's bogies based on the discrete phase model, J. Applied Fluid Mechanics 10(6), 1729–1745. doi: 10.29252/jafm.73.245.27410.

[6] M. Liu, et al., (2019) A numerical study of snow accumulation on the bogies of high-speed trains based on coupling improved delayed detached eddy simulation and discrete phase model, J. Rail and Rapid Transit 233(7), 715–730. doi: 10.1177/0954409718805817.

[7] H. Yoon, S. Min, K. Yee (2019) A study on estimation of snow collection efficiency on train bogie with respect to the characteristics of snow. Korean J. Comput. Fluids Eng 24(4), 43–53. doi: 10.6112/kscfe.2019.24.4.043.

[8] L. Cai, Z. Lou, T. Li, J. Zhang (2021) Numerical study of dry snow accretion characteristics on the bogie surfaces of a high-speed train based on the snow deposition model, Int. J. Rail Transportation 10(3), 393–411. doi: 10.1080/23248378.2021.1918589.

[9] K. Nishimura, J. Hunt (2000) Saltation and incipient suspension above a flat particle bed below a turbulent boundary layer, J. Fluid Mechanics 417, 77–102. doi: 10.1017/S0022112000001014.

[10] A. Vigano (2012) Experimental and numerical modeling of wet snow accretion on structures, Doctoral dissertation, ISAE-ENSMA National School of Mechanics and Aerotechnique. url: https://tel.archives-ouvertes.fr/tel-00786189.

[11] H. El-Batsh, H. Haselbacher (2000) Effect of turbulence modeling on particle dispersion and deposition on compressor and turbine blade surfaces, Proceedings

of ASME turbo expo 2000: power for land, sea, and air 1: Aircraft Engine; Marine; Turbomachinery, V001T03A084. doi: 10.1115/2000-GT-0519.

[12] T. Sato, K. Kosugi, S. Mochizuki, M. Nemoto (2008) Wind speed dependences of fracture and accumulation of snowflakes on snow surface, Cold Regions Science and Technology 51, 229–239. doi10.1016/j.coldregions.2007.05.004.

[13] L. Makkonen (2000) Models for the growth of rime, glaze, icicles and wet snow on structures, Phil. Trans. R. Soc. Lond. A 358, 2913–2939. doi: 10.1098/rsta.2000.0690.

[14] Y. Sakamoto (2000) Snow accretion on overhead wires. Phil. Trans. R. Soc. Lond. A 358, 2941–2970. doi: 10.1098/rsta.2000.0691.

[15] P. Admirat (2008) Wet snow accretion on overhead lines, Atmospheric icing of Power Networks, Springer Netherlands, 119–169. doi: 10.1007/978-1-4020-8531-4_4.

[16] B.E.K. Nygaard, H. Ágústsson, K. Somfalvi-Tóth (2013) Modeling wet snow accretion on power lines: Improvements to previous methods using 50 years of observations, Journal of Applied Meteorology and Climatology 52, 2189–2203. doi: 10.1175/JAMC-D-12-0332.1.

[17] K. Yamamoto, et al. (2020) Evaluation for characteristics of wet snow accretion on transmission lines - establishment of a experimental method using a vertical plate. Cold Regions Science and Technology 174, 103014. doi: 10.1016/j.coldregions.2020.103014.

[18] B. Mohammadian (2021) Interfacial phenomena in snow from its formation to accumulation and shedding, Advances in Colloid and Interface Science 67(265), 847–861. doi: 10.1016/j.cis.2021.102480.

[19] V.T.J. Phillips, et al. (2015) A parameterization of sticking efficiency for collisions of snow and graupel with ice crystals: Theory and comparison with observations, Journal of the atmospheric sciences 72(12), 4885–4902. doi: 10.1175/JAS-D-14-0096.1.

[20] W.G. Ji, et al. (2021) Establishment of small climate wind tunnel for snowfall. Journal of the Korean Society for Railway 24(10), 876–887. doi: 10.7782/JKSR.2021.24.10.876.

[21] S.H. Seo, W.G. Ji, J.W. Jeong, K.H. Kim (2021) Experimental investigation on effect of surface heat transfer to snow accretion under dry snow condition, Journal of the Korean Society for Railway 24(11), 921–930. doi:

10.7782/JKSR.2021.24.11.921.

[22] Dantec Dynamics® (2022) Measurement principles of piv, access date: 15 July 2022. url: https://www.dantecdynamics.com/solutions-applications/solutions/fluid-mechanics/particle-image-velocimetry-piv/measurement-principles-of-piv/

[23] Scarano (2013) Tomographic piv: principles and practice, Meas. Sci. Technol. 24, 012001. doi: 10.1088/0957-0233/24/1/012001.

[24] S. Schleef, et al. (2014) An improved machine to produce nature-identical snow in the laboratory, Journal of Glaciology 60(219), 94–102. doi: 10.3189/2014JoG13J118.

[25] J. Wåhlin, A.K. Paste, 2015. The effect of common de-icing chemicals on the hardness of compacted snow, Cold Regions Science and Technology 109, 28–32. doi: 10.1016/j.coldregions.2014.09.007.

[26] M. Lombardo, M. Schneebeli, H. Löwe (2021) A casting method using contrast-enhanced diethylphthalate for micro-computed tomography of snow, Journal of Glaciology 67(265), 847–861. doi: 10.1017/jog.2021.35.

[27] F. Nilsson, et al. (2019) Modelling anti-icing of railway overhead catenary wires by resistive heating, Int. J. Heat and Mass Transfer 143, 118505. doi 10.1016/j.ijheatmasstransfer.2019.118505.

[28] Y.L. Sant, M. Marchand, P. Millan, J. Fontaine (2002) An overview of infrared thermography techniques used in large wind tunnels, Aerospace Science and Technology 6, 355–366. doi: 10.1016/S1270-9638(02)01172-0.

[29] E. Sparrow, J. Abraham, J. Tong (2004) Archival correlations for average heat transfer coefficients for non-circular and circular cylinders and for spheres in cross-flow, Int. J. Heat and Mass Transfer 47, 5285–5296. doi: 10.1016/j.ijheatmasstransfer.2004.06.024.

[30] K. Kawashima, T. Endo, Y. Takeuchi (1998) A portable calorimeter for measuring liquid-water content of wet snow, Annals of Glaciology 26, 103–106. doi: 10.3189/1998AoG26-1-103-106.

[31] G. Wakahama, D. Kuroiwa, K. Gotō (1977) Snow accretion on electric wires and its prevention, Journal of Glaciology 19(81), 479–487. doi: 10.3189/S0022143000215682.

[32] T. Sato, K. Kosugi, A. Sato (2001) Saltation-layer structures of drifting snow observed in wind tunnel, Annals of Glaciology 32, 203–208. doi:

10.3189/172756401781819184.

[33] M. Farzaneh, C. Volat, A. Leblond (2008) Anti-icing and deicing techniques for overhead lines, Atmospheric Icing of Power Networks, Springer Netherlands, 229–268. doi: 10.1007/978-1-4020-8531-4_6.

[34] R. Hefny, et al. (2009) Adhesion of wet snow to different cable surfaces, 13th IWAIS, 8th –11th September 2009. url: http://eprints.hud.ac.uk/id/eprint/16648

[35] S.C. Colbeck, S.F. Ackley (1982) Mechanisms for ice bonding in wet snow accretions on power lines, Proceedings of the 1st IWAIS, 25–30.

[36] G. Poots, P.L.I. Skelton (1995) Thermodynamic models of wet-snow accretion: axial growth and liquid water content on a fixed conductor. Int. J. Heat and Fluid Flow 16, 43–49. doi: 10.1016/0142-727X(94)00007-Y.

[37] J. Heil, et al. (2020) Relationships between surface properties and snow adhesion and its shedding mechanisms, Applied Sciences 10(16), 5407. doi: 10.3390/app10165407.

[38] E.E. Adams, R.L. Brown (1983) Metamorphism of dry snow as a result of temperature gradient and vapor density differences, Annals of Glaciology 4, 3–9. doi: 10.3189/S0260305500005140.

[39] D.A. Miller et al. (2003) A microstructural approach to predict dry snow metamorphism in generalized thermal conditions. Cold Regions Science and Technology 37, 213–226. doi: 10.1016/j.coldregions.2003.07.001.

[40] M. Farzaneh, K. Savadjiev (2008) Statistical analysis of icing event data for transmission line design purposes, Atmospheric Icing of Power Networks, Springer Netherlands, 31–81. doi: 10.1007/978-1-4020-8531-4_2.

[41] F.W. Murray (1967) On the computation of saturation vapor pressure. J. Applied Meteorology and Climatology 6, 203–204. doi: 10.1175/1520-0450(1967)006<0203:OTCOSV>2.0.CO;2.

[42] G. Poots, P.L.I. Skelton (1994) Simple models for wet-snow accretion on transmission lines: snow load and liquid water content, Int. J. Heat and Fluid Flow 16, 411–417. doi: 10.1016/0142-727X(94)90055-8.

[43] T.C. Currie, D. Fuleki, D.C. Kenzevici, J.D. Macleod (2013) Altitude scaling of ice crystal accretion, 5th AIAA Atmospheric and Space Environments Conference, San Diego, USA, 2677.

국문 초록

겨울철 착설로 인해 대차부 및 열차 하부에 형성된 눈더미는 철도차량의 성능저하와 함께 다양한 형태의 피해를 유발한다. 철도 차량의 착설 현상에 적용 가능한 신뢰할 수 있는 눈 입자 및 표면 계면의 부착 특성과 그 원인을 규명하기 위해선, 기계적 또는 전기적 시스템에서 발생하는 표면 열 전달의 영향을 고려해야 한다. 본 논문에서는 소형 기후 풍동을 이용하여 영하의 기온에서 발생하는 건설 부착 특성을 이해하기 위해 풍동 실험 및 가열된 표면에 대한 건형 착설 모델링을 수행하였다. 풍동 실험은 기온, 풍속, 적설량과 같은 대기 조건 및 표면 열전달의 영향을 관찰하기 위해 체계적으로 실험 조건이 설정되었다. 정교한 측정 과정을 통해 착설층 성장 속도, 부착성 계수 및 함습률과 같은 물성치가 획득되었으며, 가열 표면에 대한 건형 착설 현상의 매커니즘이 분석되었다. 실험 결과 착설 과정에서 표면 열전달은 강한 영향력을 보여주었다. 건설의 부착성 계수는 착설층의 함습률 및 기상 매개변수와 강한 상관관계를 보였다. 착설층의 함습률이 40%에 도달하였을 때 착설층은 표면으로부터 떨어지는 것으로 나타났다. 착설층의 부착성 계수와 함습률은 착설층 내부의 증발 및 응축, 대류 냉각 그리고 눈의 융해가 고려된 열역학적 모델링을 통해 추정되었다. 모델링 결과는 실험 측정값과 분석 및 교차검증 되었으며, 부착성 계수 및 함습률에 대해 수정결정계수는 각각 0.97과 0.92로 나타났다. 본 연구의 실험적, 해석적 분석 결과는 착설 현상에 대한 기존 지식을 건설의 영역으로 확장한 것으로 볼 수 있다. 따라서 본 연구 결과는 습설, 단열 표면 조건 등 다양한 열역학적 조건으로 확장 및 적용될 수 있다.

주요어 : 착설 현상, 건설, 풍동 시험, 표면 열전달, 부착성 계수, 함습률
학 번 : 2020-29410